Aditi Singh

Postdoctoral Fellow · Osterweil Lab · Next-Gen Accelerator Grant Awardee (2025)

Affiliation: Rosamund Stone Zander and Hansjoerg Wyss Translational Neuroscience Center · F. M. Kirby Neurobiology Center, Boston Children's Hospital, Harvard Medical School

Department: Neurology

Labs: Osterweil Lab

Authors: Aditi Singh & Emily K. Osterweil

Preprint: Singh et al., *FMR1 reduction alters cellular and circuit properties in human cortex. preprint* bioRxiv 2026, doi:10.64898/2026.03.11.711123

Cross-species comparison of molecular changes in Fragile X syndrome

Single-cell RNA-seq of FMR1-deficient human cortical slices, and how their transcriptomic changes compare with Fragile X patient cortex and the Fmr1 knockout mouse.

Introduction

Fragile X syndrome (FXS) is the most common inherited cause of intellectual disability and a leading monogenic cause of autism. It arises when *FMR1* is transcriptionally silenced and neurons lose FMRP, an RNA-binding protein that regulates translation, mRNA stability and transport. Most of what we know about how FMRP loss changes the cortex comes from the *Fmr1* knockout (KO) mouse, but human and mouse cortex differ in cell types, connectivity and physiology, and FMRP binds different transcripts in human and mouse neurons. Because people with FXS rarely undergo brain surgery, these differences have been hard to study in living human tissue.

To study these differences directly, we acutely reduced *FMR1* in human cortical tissue. Organotypic slices were prepared from non-lesional cortex removed during pediatric epilepsy surgery, and adjacent slices from each resection were transduced with an AAV carrying either an *FMR1* shRNA (sh*FMR1*) or a scrambled shRNA (shScr). Both constructs express mCherry from a neuron-specific synapsin promoter. Seven days after transduction, *FMR1* mRNA in sorted neurons was reduced by more than 80% and FMRP protein by more than half.

We next generated single-cell RNA-seq from FACS-purified neurons in paired shScr and sh*FMR1* slices from three donors. This vignette describes how we built and quality-controlled that dataset, and how we compared it with published data from FXS patient cortex and the *Fmr1*-KO mouse. Results are from our preprint, which has not yet been peer reviewed.

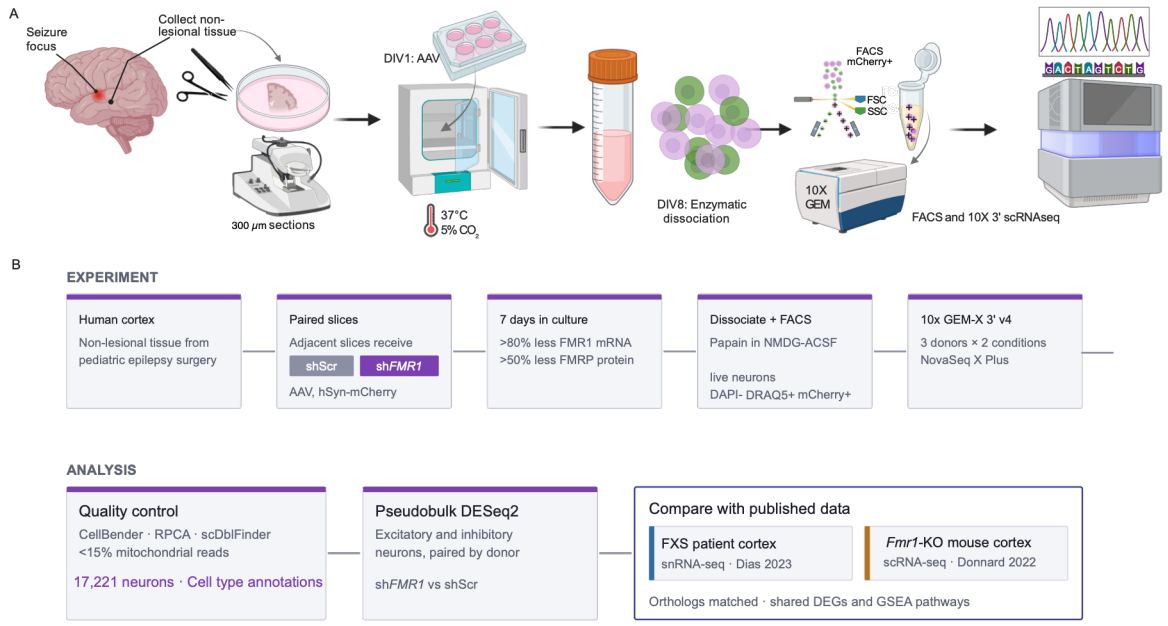


Figure 1. Experimental workflow and analysis strategy. (a) Non-lesional cortex collected during pediatric epilepsy surgery was cut into 300 µm organotypic slices. On day in vitro (DIV) 1, adjacent slices were transduced with AAVs expressing scrambled (shScr) or *FMR1*-targeting (sh*FMR1*) shRNA, together with mCherry driven by the human synapsin promoter, and cultured at 37 °C in 5% CO_2. On DIV8, slices were enzymatically dissociated, and live transduced neurons ($DAPI^-$ $DRAQ5^+$ $mCherry^+$) were isolated by FACS for 10x Genomics GEM-X 3' single-cell RNA-seq. (b) Summary of the experiment and analysis. Paired shScr and sh*FMR1* samples from three donors were sequenced, and the data were filtered (CellBender, RPCA integration, scDblFinder, <15% mitochondrial reads) to 17,221 annotated neurons. Pseudobulk differential expression (DESeq2, s*hFMR1* vs shScr, paired by donor) in excitatory and inhibitory neurons was compared with published single-nucleus RNA-seq from FXS patient cortex (Dias et al., 2023) and single-cell RNA-seq from *Fmr1*-KO mouse cortex (Donnard et al., 2022), after matching orthologous genes. *Created with BioRender.com.*

Preparation of single-cell libraries from human cortical slices

We chose whole cells over nuclei because FMRP acts in the cytoplasm, where it controls transcript stability and translation, and nuclear RNA would miss much of that. The trade-off is that adult human neurons are fragile after a week in culture, so most of our optimization went into dissociation and sorting.

Each 300 µm slice was digested for 30 minutes at 37 °C in papain (20 U/mL) prepared in an NMDG-based ACSF with DNase and RNase inhibitor. It was then triturated through fire-polished pipettes of decreasing bore and filtered at 70 µm. Before sorting we stained cells with DRAQ5 to mark intact nucleated cells, and added DAPI immediately before the sort to exclude dead cells. On a BD FACSAria with a 100 µm nozzle at low pressure, we gated singlets by scatter and collected $mCherry^+$ $DRAQ5^+$ $DAPI^-$ neurons into 20-30 µL, small enough to load 10x channels

at the recommended concentration. The DRAQ5^{+} fraction of the cell gate ranged over 75% across the six samples.

Libraries were made with the Chromium GEM-X Single Cell 3′ v4 kit, targeting about 5,000 cells per channel, and sequenced on an Illumina NovaSeq X Plus. The shScr and sh*FMR1* samples from each donor were always sorted, loaded and sequenced together, so donor and batch effects are shared across each pair.

Processing and quality control

Reads were aligned to GRCh38 with Cell Ranger 8.0.1. Sorted cell suspensions carry ambient RNA released by damaged cells, so we ran CellBender on each sample before anything else. Samples were then integrated in Seurat with reciprocal PCA, doublets were called with scDblFinder, and cells with 15% or more mitochondrial reads were removed. Finally, we dropped clusters that had no clear marker expression or fewer than 100 cells across both conditions. Table 1 shows how many cells survived each step.

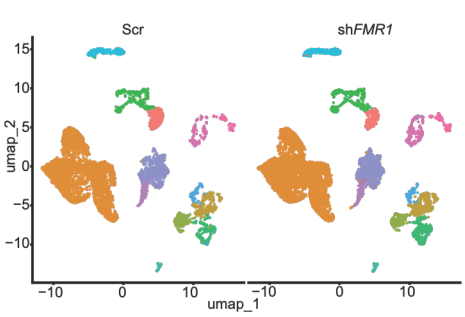
Table 1. Cells retained at each processing step.

Step	Cells
Called by Cell Ranger (6 samples, 3 donors)	25,953
After CellBender and RPCA integration	18,773
After doublet removal and <15% mitochondrial reads	17,441
After removing clusters without clear markers or <100 cells	17,221
Final: shScr / sh*FMR1*	**7,438 / 9,783**

Cell-type annotation

We annotated cells in two steps. First, we transferred labels from an age-matched human temporal cortex atlas (Steyn et al., 2024) using Seurat anchors and projected cells onto the reference UMAP. Then we refined subtypes with canonical markers. This gave nine excitatory types spanning layers 2/3 to 6 and four inhibitory groups: VIP, SST/PV, and two CGE-derived populations. One CGE group appeared immature, which probably reflects the donors' young age. As in other human cortex datasets, layer 2/3 excitatory neurons were the largest population (Figure 2).

Every cell-type was present in both conditions, so we could compare expression within each type using pseudobulk DESeq2, pairing samples by donor.



Number of cell in each cluster per condition

Cell_types	Scr	sh*FMR1*
Exc_L2/3_LAMP5_ETV1	349	340
Exc_L2/3_CUX1_LAMP5	4167	4702
Exc_L2/4_CUX2_RORB	339	590
Exc_L4_RORB_CLSTN2	320	209
Exc_L4_RORB_PAX6	358	592
Exc_L4/6_RORB_TSHZ2	206	611
Exc_L5/6_ETV1_FEZF2	38	73
Exc_L5/6_TLE4	232	498
Exc_L6_TLE4_CLSTN2	103	144
Inh_CGE_ADARB2-high	900	1098
Inh_CGE2_ADARB2-low	197	196
Inh_SST_PV	156	433
Inh_VIP	73	297

Figure 2. Neuronal cell types in shScr and sh*FMR1* slices. Left, UMAPs of shScr and shFMR1 neurons colored by annotated cell type. Right, number of cells per type and condition, pooled across three donors. [Adapted from Singh et al., bioRxiv 2026, Fig. S4]

Comparing human slices, FXS patients and the mouse

To ask whether acute *FMR1* reduction in human slices resembles the disease, we compared our results with single-nucleus RNA-seq from FXS patient and control cortex (Dias et al., 2023). To benchmark that comparison, we ran the same analysis on single-cell RNA-seq from *Fmr1*-KO and wild-type mouse cortex (Donnard et al., 2022). The mouse, like patients, lacks FMRP from before birth, while our slices are an acute knockdown in cortex that has already developed.

The two published datasets have far fewer cells and replicates per subtype than ours, so we summarized all three into two classes, excitatory and inhibitory neurons, before comparing them. Mouse genes were mapped to human orthologs. For each comparison, we asked what fraction of the genes changed in patients were also changed in each model, and whether that overlap was greater than expected by chance. Because overlaps of thresholded gene lists depend on statistical power, we also compared pathways using gene set enrichment analysis (GSEA).

Human slices shared more of the patient signature than the mouse did (Figure 3). In excitatory neurons, 31.2% of the genes changed in FXS patients were also changed in sh*FMR1* slices, against 13.4% for the mouse. In inhibitory neurons, the figures were 14.2% and 10.5%. Both slice overlaps were significantly greater than chance; neither mouse overlap was. At the pathway level, 27.2% of patient excitatory-neuron pathways were also changed in slices, against 6.47% in the mouse, with 19.4% and 4.79% in inhibitory neurons.

Among the genes changed in both slices and patients were ion-channel subunits that play role in neuronal excitability. Pathways shared by slices and patients included vesicle trafficking, monoatomic ion transport and protein maturation.

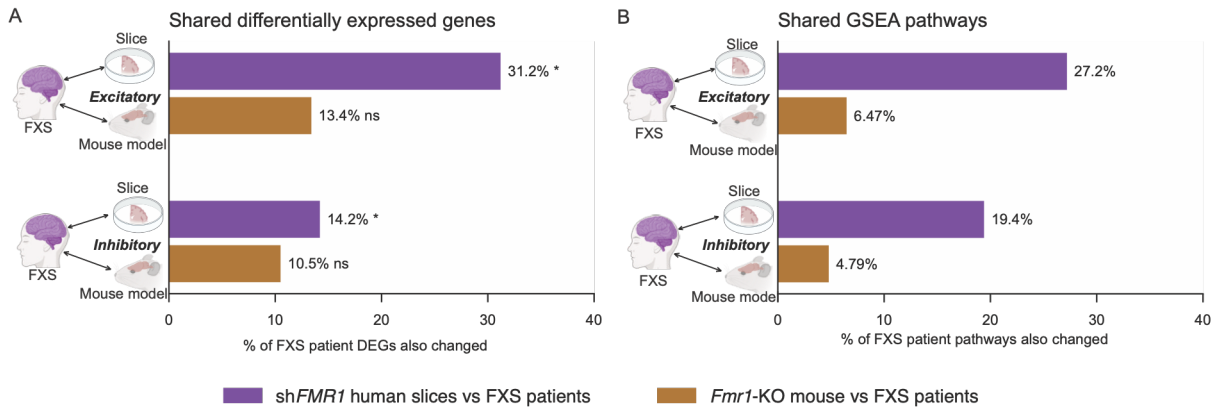


Figure 3. FMR1-deficient human slices share more of the FXS patient signature than the Fmr1-KO mouse. *(A) Percent of genes significantly changed in FXS patient neurons that are also changed in each model. * overlap greater than expected by chance; ns, not significant. (B) Percent of GSEA pathways enriched in FXS patient neurons that are also enriched in each model. Values from the bioRxiv preprint (Singh et al., 2026). Icons created with BioRender.com.*

Limitations

These comparisons have limits. The published reference datasets are small: the FXS patient data come from only two FXS donors, and the *Fmr1*-KO mouse data from three knockout and three wild-type animals, which called relatively few significant genes. With so few samples, some real changes in patients or mice are likely missed, and the overlap percentages should be read as estimates. Within our own data, interneurons were underrepresented compared with excitatory neurons. This probably reflects their lower abundance in cortex and their sensitivity to dissociation. As a result, we could not compare individual interneuron subtypes such as PV and SST across datasets, and pooled them into a single inhibitory class.

Data availability and future plans

Processed differential expression results will be released with the publication as supplementary tables, and raw data will be deposited in dbGaP at that The FXS patient single-nucleus data (Dias et al., 2023) were shared with us by the authors. The *Fmr1*-KO mouse single-cell data (Donnard et al., 2022) are publicly available from GEO (GSE147191).

Acknowledgments

We thank the patients and families who donated tissue; Ryan Guardado, Remi Hirsh and Elizabeth Buttermore for help with tissue collection; and Christopher A. Walsh and Caroline M. Dias for sharing the FXS patient data. Experiments used the IDDRC core facilities at Boston Children's Hospital (NIH P50 HD105351), including the Repository Core for Neurological Disorders and the Flow Cytometry Core. The Cell Discovery Network Next-Gen Accelerator Grant supported the pilot for single-cell library preparation and sequencing.

References

1. Singh A, Abbaspoor S, Chung L, Heinrich MJ, et al., Farrell JS, Osterweil EK. *FMR1* reduction alters cellular and circuit properties in human cortex. bioRxiv 2026. doi:10.64898/2026.03.11.711123
2. Dias CM, Issac B, Sun L, et al., Walsh CA. Glial dysregulation in the human brain in fragile X-associated tremor/ataxia syndrome. PNAS 2023;120:e2300052120.
3. Donnard E, Shu H, Garber M. Single cell transcriptomics reveals dysregulated cellular and molecular networks in a fragile X syndrome model. PLoS Genet 2022;18:e1010221.
4. Steyn C, Mishi R, Fillmore S, et al., Hockman D. A temporal cortex cell atlas highlights gene expression dynamics during human brain maturation. Nat Genet 2024;56:2718–2730.
5. Shen M, Sirois CL, Guo Y, et al., Zhao X. Species-specific FMRP regulation of RACK1 is critical for prenatal cortical development. Neuron 2023;111:3988–4005.
6. Fleming SJ, Chaffin MD, Arduini A, et al., Babadi M. Unsupervised removal of systematic background noise from droplet-based single-cell experiments using CellBender. Nat Methods 2023;20:1323–1335.
7. Germain PL, Lun A, Garcia Meixide C, Macnair W, Robinson MD. Doublet identification in single-cell sequencing data using scDblFinder. F1000Research 2021;10:979.
8. Hao Y, Stuart T, Kowalski MH, et al., Satija R. Dictionary learning for integrative, multimodal and scalable single-cell analysis. Nat Biotechnol 2024;42:293–304.
9. Love MI, Huber W, Anders S. Moderated estimation of fold change and dispersion for RNA-seq data with DESeq2. Genome Biol 2014;15:550.